Article

A Straightforward Electrochemical Approach for the Simultaneous Determination of Thymol and Carvacrol in Essential Oils

Sabrina Antonella Maccio [1,2], Ruben Darío Alaniz [1,2], Gastón Darío Pierini [1,2], María Alicia Zon [1,2,†], Fernando Javier Arévalo [1,2], Héctor Fernández [1,2], Héctor Casimiro Goicoechea [2,3], Sebastian Noel Robledo [2,3,*] and Mirta Raquel Alcaraz [2,4,*]

[1] Departamento de Química, Grupo GEANA, Instituto para el Desarrollo Agroindustrial y de la Salud (IDAS), Facultad de Ciencias Exactas, Físico-Químicas y Naturales, Universidad Nacional de Río Cuarto, Rio Cuarto 5800, Argentina; smaccio@exa.unrc.edu.ar (S.A.M.); gpierini@exa.unrc.edu.ar (G.D.P.); farevalo@exa.unrc.edu.ar (F.J.A.)

[2] Consejo Nacional de Investigaciones Científicas y Técnicas (CONICET), Godoy Cruz 2290, Argentina; hgoico@fbcb.unl.edu.ar

[3] Departamento de Tecnología Química, Grupo GEANA, Instituto para el Desarrollo Agroindustrial y de la Salud (IDAS), Facultad de Ingeniería, Universidad Nacional de Río Cuarto, Rio Cuarto 5800, Argentina

[4] Laboratorio de Desarrollo Analítico y Quimiometría (LADAQ), Facultad de Bioquímica y Ciencias Biológicas, Universidad Nacional del Litoral, Ciudad Universitaria, Santa Fe S3000ZAA, Argentina

* Correspondence: srobledo@ing.unrc.edu.ar (S.N.R.); malcaraz@fbcb.unl.edu.ar (M.R.A.)

† to the memory of María Alicia Zon.

Abstract: A novel, simple, rapid, and non-expensive analytical method based on square wave voltammogram at Pt-microelectrode coupled with partial least square multivariate calibration was used for the simultaneous quantitation of thymol (THY) and carvacrol (CAR) in thyme and oregano essential oils. Results demonstrated that the multivariate calibration method successfully exploited the first-order advantage, rendering highly satisfactory quantitative figures (average recoveries not statistically different than 100%). Moreover, the results agree well with those obtained from the official analytical method. Last, the method's environmental sustainability was asserted using the AGREE metric, highlighting its eco-friendly nature. More importantly, the proposed analytical procedure does not require previous sample preparation or electrode surface modification. The results underscore the suitability of the method for determining THY and CAR in essential oils at low concentrations (LOD ~ 7.6 µM) with REP% below 5.6%, meeting the requirements of the green analytical chemistry.

Keywords: thymol; carvacrol; Pt-microelectrode; essential oils; partial least squares

1. Introduction

Thymol (2-iso-propyl-5-methylphenol (THY)) and carvacrol (2-methyl-5-iso-propyl-phenol (CAR)) are phenolic monoterpenes and position isomers (Figure 1) that have several biological effects. THY have demonstrated high efficacy in controlling pigeon coccidiosis [1], produced growth inhibition of bacteria such as Staphylococcus aureus, Pseudomonas aeruginosa, and Escherichia coli [2], and caused the inactivation of Alicyclobacillus acidoterrestris in fruit juice [3], among many others [4,5]. CAR also shows biological effects such as the strong inhibition effect on the activity of xanthine oxidase [6], neuroprotective effects in cerebral ischemia [7], hepatoprotective role against ethanol-induced liver toxicity [8], and several others. They have also been used as natural antioxidants for food preservation [9]. These compounds are two principal constituents of thyme and oregano essential oil (TEO and OEO, respectively) [10–13], providing them with particular biological properties [14,15], such as antifungal, antiviral, antitumor, and anti-inflammatory activities [16–18].
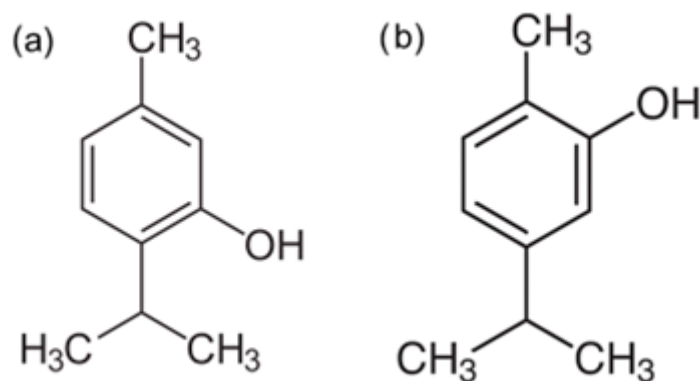
Figure 1. Chemical structures of thymol (**a**) and carvacrol (**b**).

Nowadays, several methods have been developed aiming for the simultaneous determination of THY and CAR, which are mainly based on liquid chromatography (LC) techniques with UV or fluorescence detection [19–22], gas chromatography–mass spectrometry (GC-MS) [23–27] and tandem mass spectrometry (GC-MS/MS) [28], GC coupled with flame ionization detector (GC-FID) [29], and ultraperformance convergence chromatography (UPC) [30]. Although these methods exhibit high accuracy and sensitivity, they are usually time-consuming, involve significant solvent consumption, generate large amounts of waste, and require intricate sample preparation [31]. In this regard, electrochemical methods emerge as a straightforward and inexpensive alternative, offering notable analytical advantages such as high accuracy, precision, sensitivity, and the possibility of miniaturization. Electroanalytical methods are tools that can be integrated into the principles of green analytical chemistry (GAC), as described by Yáñez-Sedeño et al. [32], because they provide real-time detection and in situ monitoring, positioning them as a promising alternative for determining THY and CAR.

Notwithstanding all the above characteristics, only a few reports regarding THY and CAR determination via electrochemical sensors are found in the literature, with more reporting on the individual analysis of these analytes. It is worth noticing that the simultaneous determination of THY and CAR is a troublesome challenge due to the proximity of their oxidation potentials. Hence, when both analytes are present, the concentration is generally expressed as the total content of THY and CAR. For instance, they have been jointly determined in phytotherapeutic black seed oil using differential pulse voltammetry (DPV) at glassy carbon electrode (GCE) [33] and in selected Mexican oregano essential oils using single-walled carbon nanotubes screen-printed electrodes (SWCNT-SPEs) [34]. Likewise, the total content of THY and CAR was determined by linear sweep voltammetry (LSV) at GCE in TEO and OEO samples [35].

However, novel approaches have revealed the possibility of simultaneously determining THY and CAR with the aid of chemometrics. Chemometric tools play an essential role in electroanalysis [36], principally for multianalyte calibration and modeling in multicomponent dynamic systems [37–40]. Multivariate data analysis is a method of examining data comprising multiple variables derived from a number of samples. The objective of this approach is to identify all the variations present in the data matrix under study. Consequently, chemometric tools are employed to ascertain the relationships between the samples and variables within a given data set and to transform them into new latent variables [41]. Multivariate calibration methods have gained widespread acceptance due to their ability to analyze the interactions between analytes. In this context, the partial least squares (PLS) algorithm is the most preferred tool among chemometricians for developing calibration models for analyzing big numbers of data sets in a rapid and efficient manner [42]. In these regards, an electrochemical method based on square wave voltammetry (SWV) at GCE coupled with artificial neural network (ANN) analysis [43] and a strategy using DPV at boron-doped diamond (BDD) electrodes with regression [44] were successfully developed for the simultaneous determination of THY, CAR, and eugenol in honey samples. More

recently, CAR was determined in the presence of high THY concentrations through a multi-way calibration model demonstrating the potential of combining electrochemical second-order data with chemometrics [45].

Under the IUPAC definition, a microelectrode is an electrode with tens of micrometers or fewer dimensions. This small dimension has several significant practical implications, including a decreased ohmic drop of potential, IR, the rapid establishment of a steady-state signal, increased current due to enhanced mass transport at the electrode boundary, and an increased signal-to-noise ratio. Consequently, this microelectrode is advantageous in numerous areas of electroanalytical chemistry, especially in organic media [46].

This work presents an electroanalytical methodology for the simultaneous determination of THY and CAR in TEO and OEO by applying SWV on Pt-microelectrode (PtME) coupled with chemometric tools such as multivariate calibration based on PLS, thereby achieving integrated development with GAC principles.

2. Materials and Methods

2.1. Reagents

Carvacrol (CAR, $\geq$98%) and thymol (THY, 99%) standards, tetrabutylammonium perchlorate (TBAP, $\geq$99.0%), and oregano and thyme essential oil samples (OEO and TEO) were obtained from Sigma–Aldrich (Darmstadt, Germany). Acetonitrile (ACN, HPLC grade) was purchased from Sintorgan (Buenos Aires, Argentina) and kept over 3 Å molecular sieves to minimize the water content in organic solvent to trace levels. Ethanol (EtOH) was purchased from Sintorgan (Buenos Aires, Argentina). All reagents were used as purchased.

CAR and THY stock solutions (15 mM) were prepared in ethanol (EtOH) and kept at 4 °C in darkness.

2.2. Instrumentation

Voltammetric measurements were performed with an Epsilon potentiostat (BASi-Bioanalytical System, West Lafayette, IN, USA) using the electrochemical analysis software provided by the manufacturer. The working electrodes were a platinum disk microelectrode (PtME, BASi Electroanalytical System, USA, diameter = 10 μm) and platinum macroelectrode, the counter electrode was a large-area platinum foil (A ~ 2 cm^2), and the reference electrode was Ag/AgCl (3 M NaCl). For the measurements, the electrodes were inserted into the electrochemical cell (approx. 2.0 mL volume) through holes in its Teflon cover.

The chemical composition of EOs was determined by the reference method based on gas chromatography–mass spectrometry (GC-MS), using a Perkin Elmer Clarus 600 equipment (Shelton, CT, USA) with a Perkin Elmer column DB5 (30 m, 0.25 mm ID, 0.25 μm) operating in temperature gradient mode. The gradient was established as follows: at the beginning, the oven was set at 60 °C for 5 min, and then it was gradually increased from 60 °C to 240 °C at a rate of 5 °C min^{-1}; finally, it was kept constant at 240 °C for 10 min. The carrier gas (Helium) flow was 1 mL min^{-1}, and the injector temperature was 300 °C, operating in splitless mode. Before injection, samples were diluted in hexane (1/100). The analysis was performed in scan mode, from m/z = 50 to m/z = 350 (scan time: 0.2 s, inter-scan time: 0.1 s), solvent delay: 5 min. The main components were identified by directly comparing the retention time and the mass spectrum EO components with the pure standard compounds. Relative concentrations were calculated according to peak area normalization given by TurboMass 5.4.2. software [47].

2.3. Voltammetry Measurements

Before measurement, the PtME surface was stabilized, aiming to produce an electrochemical activation of the electrode surface, allowing reproducible responses [48]. This stage involved recording CV from 0.0 V to 2.0 V (vs. Ag/AgCl (3 M NaCl)) at a scan rate (ν) of 0.100 V s^{-1} in ACN + 0.1 M TBAP solution. Then, SWV signals were recorded in the potential range of 0.9 V to 2.2 V. For SWV, the square wave amplitude (ΔE_{sw}) was 0.025 V,

using a step potential (ΔEs) and a frequency (f) of 0.005 V and 15 Hz, respectively. All the experiments were carried out at room temperature.

2.4. Estimation of ME Electroactive Area

The electroactive area of the PtME disk was determined following the procedure reported by the Compton group [49], in which a double potential step chronoamperometry in ACN + 0.1 M TBAP solution, using the ferrocene/ferrocenium ion (Fc/Fc$^+$) as the redox couple, is implemented. The current–time responses were recorded after applying a potential of 0.0 V (where the faradaic process does not occur) for 10 s. Then, the potential was maintained at 0.6 V (where the faradaic reaction occurs at the maximum possible rate) for 5 s. Finally, the potential was returned to its initial value for 5 s. The responses were analyzed using the Shoup and Szabo equations [50].

2.5. Calibration and Validation Samples

The calibration sample set was designed using a multilevel multifactor design [51] and involved a series of two-component mixtures at five concentration levels. In this way, twenty-five standard solutions, covering the concentration range of 92 μM to 1380 μM for THY and 93 μM to 1420 μM for CAR. The lower and upper concentration limits were established considering the expected concentration of the analytes in the EO samples. A validation set of 16 synthetic mixtures was prepared with random concentrations in the ranges defined by the extremes of a calibration set. The different concentrations of the calibration and prediction sets are shown in Table S1 (Supplementary Materials).

All the solutions were prepared by transferring proper aliquots of the stock solutions to 5.00 mL of ACN + 0.1 M TBAP as the supporting electrolyte. Then, 2.0 mL was placed into the electrochemical cell for measurements.

2.6. Essential Oil Samples

TEO and OEO commercial essential oils were analyzed. Initial EO stock solutions were prepared by diluting 50 μL of each commercial EO with EtOH, reaching a final volume of 5 mL, and stored at 4 C until analysis.

Two groups of 4 samples, comprising both blank and spiked samples, were analyzed to create a set of EO samples. Using a randomized design approach, aliquots from the EO stock solution were spiked with THY and CAR at different concentration levels. The solutions were prepared by transferring the appropriate aliquots of each analyte solution into 5.0 mL of the EO stock solution. (For more information, the reader is referred to Table S2, Supplementary Materials).

For measurement purposes, 0.5 mL of the blank or spiked EO sample was transferred to a 5.0 mL flask, completing the mark with ACN + 0.1 M TBAP. Finally, 2.0 mL of the resulting solution was placed in the electrochemical cell for analysis.

2.7. Software

Data processing and analysis were performed in MATLAB 2015b [52]. PLS algorithm was implemented in MVC1 [53], for which the MATLAB codes are available at https://data.mendeley.com/datasets/8f7kmx7msk/1 (accessed on 5 Feburary 2024). The version of Green used was the AGREE standalone software, which was freely downloaded from https://mostwiedzy.pl/wojciech-wojnowski,174235-1/AGREE (accessed on 8 July 2024) [54].

3. Results and Discussion

3.1. The Electrochemical Behavior of THY and CAR

The influence of the scan rate (v) on the THY and CAR electrochemical responses was studied by cyclic voltammetry (CV). Figure S1a,b (Supplementary Materials) show the cyclic voltammograms recorded at Pt macroelectrode in ACN + 0.1 M TBAP for a THY concentration of 1.0×10^{-3} M and CAR concentration of 1.0×10^{-3} M, respectively. Therefore, the anodic peak current ($I_{p,a}$) for the THY and CAR oxidation peak increases as

v increases. Figure S1c,d (Supplementary Materials) show the corresponding $I_{p,a}$ vs. $v^{1/2}$ plots for a THY and CAR, respectively; both graphs are linear. These results allow inferring that the electron transfer process undergoes a pure diffusion-controlled process [55]. Thus, the utilization of an ultramicroelectrode can enhance the efficacy of the methodology [56].

First, the PtME was electrochemically characterized by evaluating the electrochemical oxidation of Fc to Fc^+ in ACN, as suggested in Ref [48]. Figure S2a,b (Supplementary Materials) show the cyclic voltammogram recorded at PtME at $v = 5$ mV s^{-1} and the double potential step chronoamperometry, respectively, for a Fc concentration of 3.0 mM in ACN + 0.1 M TBAP. In these conditions, the electroactive diameter electrode calculated for the PtME was (13.2 $\pm$ 0.2) μm.

Figure S3 (Supplementary Materials) displays the SW voltammograms at PtME versus Pt macroelectrode in ACN + 0.1 M TBAP for a THY and CAR concentration of 1.0×10^{-3} M in terms of current density (J, for the estimation of ME electroactive area, see Section 2.4). As expected, J is markedly elevated in PtME, thereby rendering it the optimal choice for the working electrode.

The PtME repeatability was calculated as the relative standard deviation (RSD) percentage of six independent measurements performed for 150 and 900 μM THY and CAR solutions. Calculated values were 2.41 and 2.23 for THY and CAR, respectively, when the analyte concentrations were 150 μM. RSD values were 3.05 and 3.18 for the two analytes when a concentration of 900 μM of each analyte was used.

Then, the electrochemical responses of THY and CAR were analyzed by recording the SW voltammograms at PtME in ACN + 0.1 M TBAP from 0.9 to 2.2 V using a concentration of 1400 μM and 1500 μM for THY and CAR, respectively. Figure 2 shows the SW voltammograms recorded for THY (black line), CAR (blue line), THY + CAR (red line), and the corresponding blank solution (dotted black line).
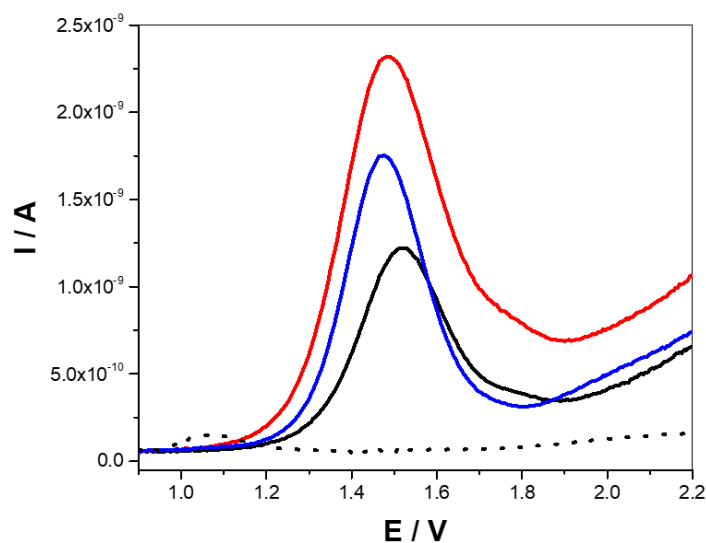
Figure 2. Square wave voltammograms for solutions of 1.4 mM THY (black line), 1.5 mM CAR (blue line), 1.4 mM THY + 1.5 mM CAR (red line), and the blank solution (dotted black line). Reaction medium: ACN + 0.1 M TBAP. Square wave conditions were $\Delta E_{SW} = 0.025$ V, $\Delta E_s = 0.005$ V, and $f = 15$ Hz.

As can be appreciated, THY shows a main oxidation peak centered at about 1.52 V, whereas the CAR oxidation peak is centered at 1.47 V. Due to the high proximity of the THY and CAR analyte oxidation potentials, the voltammetric profile of the binary mixture features one mean peak masking the individual maxima of the compounds, which precludes easily distinguishing the individual contribution of the analytes. Therefore, some resolution strategies must be performed to determine the analytes simultaneously. In this regard,

multivariate calibration models emerge as a powerful alternative, allowing the system to be mathematically resolved without requiring complicated sample treatment procedures.

3.2. Multivariate Calibration Method Development

In chemometric-based analytical methodologies, thoroughly evaluating the data properties becomes essential to designing robust data analysis protocol that ensures successful outcomes. Within the multivariate calibration framework, a critical factor is evaluating the relationship between the instrumental response and the analyte concentration. While assessing linearity, using univariate calibration models with pure analytes may prove insufficient in capturing the nuanced dynamics. This inadequacy arises due to the intricate dynamics at play when multi-analytes are present, where the linearity can undergo alterations due to competition/interaction among the electroactive species in the voltammetric measurement [57].

For linear multivariate calibration models, PLS emerges as the preferred tool. Hence, an effective method for assessing deviations from linearity involves constructing an initial PLS model with the optimal number of latent variables (LV) and predicting analyte concentrations in validation samples. Confirmation of system linearity is achieved when the LV number aligns with the number of electroactive species and the validation residuals show no correlation [58,59]. In these regards, it is worth mentioning that an increase in the LV number may arise from measurement variations between samples, which are unrelated to analyte concentration changes, thus not impacting the linear behavior of the system. Therefore, the implementation of mathematical preprocessing techniques prior to multivariate calibration becomes crucial. These techniques aid in emphasizing the data-relevant features, enhancing the predictive capability of the model in a parsimonious manner, and yielding better statistical indicators.

The raw SW voltammograms recorded for the calibration and validation samples are depicted in Figure 3. From the visual inspection, it can be noticed that these signals exhibit baseline effects that vary across the different samples. These baseline variations can be effectively mitigated by applying baseline correction methodologies or subjecting the data to mathematical transformations. One specific technique for baseline correction is the application of the Savitzky–Golay derivatives, which proved to be highly effective in eliminating baseline influences without necessitating intricate pretreatment procedures [58].
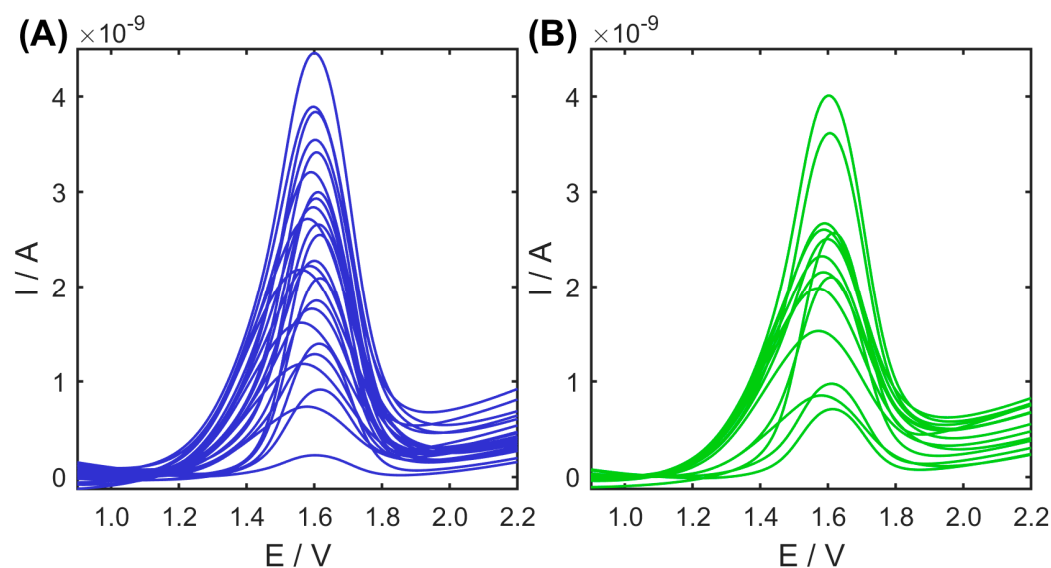
Figure 3. Raw SW voltammograms recorded for the (**A**) calibration and (**B**) validation samples at PtME, from the binary mixtures of THY and CAR, as indicated in Section 2.5. (ΔE_{SW} = 0.025 V, ΔE_s = 0.005 V, f = 15 Hz.).

Additionally, a common artifact observed is manifested as abscissa shifts between samples. This phenomenon may arise not only from differences in the analytes concentration ratio but also from stochastic empirical events commonly encountered in electrochemical data, particularly in organic media reactions where variations in ohmic drop occur due to the electrochemical cell layout, becoming significant in many cases. These events must be mitigated before applying any multivariate technique to highlight the actual contribution of the analytes. Several approaches can be utilized for abscissa shift correction; notwithstanding, it is crucial to acknowledge that implementing this strategy is not straightforward. A challenging situation may arise where the individual features of the analyte strongly overlap, rendering them indistinguishable in the global signal. In such cases, the correction process may introduce undesired effects into the data. Therefore, careful consideration and validation are paramount when applying the alignment methodologies to ensure their appropriateness for the specific characteristics of the electrochemical data under study.

In light of this scenario and aiming to develop a calibration model that more comprehensively describes the system, different strategies were evaluated and compared regarding their predictive efficacy and the robustness of the statistical indicator.

The optimized number of LVs was estimated by the well-known leave-one-out cross-validation procedure following Haaland's criterion (i.e., $p < 0.75$). Once the number of total LV was chosen, the prediction step was accomplished on the test samples. The presence of outliers in the validation samples was assessed by evaluating the spectral residues through the statistical *F*-test, which compares the squared residuals for the prediction sample and the average square residuals of the calibration set. The root-mean-squared error of prediction (*RMSEP*) and the relative error of prediction (given in %, REP%) were calculated as follows.

$$RMSEP = \sqrt{\frac{\sum_{n=1}^{N_{val}} \left(y_{nom,n} - y_{pred,n} \right)^2}{N_{val}}} \tag{1}$$

$$REP\% = 100 \frac{RMSEP}{\overline{y}} \tag{2}$$

where $y_{nom,n}$ and $y_{pred,n}$ are the nominal and predicted concentration of the analyte in the validation sample *n*, respectively, N_{val} is the total number of validation samples, and $\overline{y}$ is the mean concentration of the validation samples [58]. The results obtained for the three approaches are summarized in Table 1.

Table 1. Model parameters utilized and statistical indicators obtained for PLS models.

Analyte	Data	LV	Statistical Indicators			
			RMSECV [a] (μM)	RMSEP [b] (μM)	REP% [c]	r[2] [d]
THY	Raw	5	8.84	16.9	2.29	0.9994
	Mean-centering	4	8.84	16.9	2.29	0.9994
	First derivative [e]	3	7.95	17.0	2.30	0.9994
	Second derivative [e]	2	10.12	19.6	2.65	0.9993
CAR	Raw	5	9.04	16.5	2.17	0.9996
	Mean-centering	4	9.06	16.5	2.17	0.9996
	First derivative [e]	2	8.96	15.3	2.10	0.9996
	Second derivative [e]	2	9.05	14.8	1.95	0.9997

[a] RMSECV: root-mean-squared error of cross-validation estimated according to [58]. [b] RMSEP: root-mean-squared error of prediction estimated following Equation (1). [c] REP %: relative error of prediction given in % estimated following Equation (2). [d] r[2]: determination coefficient. [e] Mean-centering was also applied.

It is evident that models built with pretreated data require significantly fewer LV compared to raw data. This observation aligns with expectations, as pretreatment mitigates concentration-unrelated artifacts, such as baseline and abscissa shifts. The observed

satisfactory results affirm the linearity of the response–concentration behavior and indicate the absence of abscissa shifts caused by empirical variations, thus confirming the reproducibility of PtUME measurements. Although the evaluated models yielded satisfactory results with low RMSEP and REP% values below 3%, there is a preference for more parsimonious models.

To gain further insights into the predictive capability of the models, the elliptical joint of confidence region (EJCR) for the slope and the intercept of the predicted vs. nominal values plot and the prediction residuals were analyzed. Figure 4 shows the EJCR plot at a 95% confidence level and the prediction errors obtained for each model.
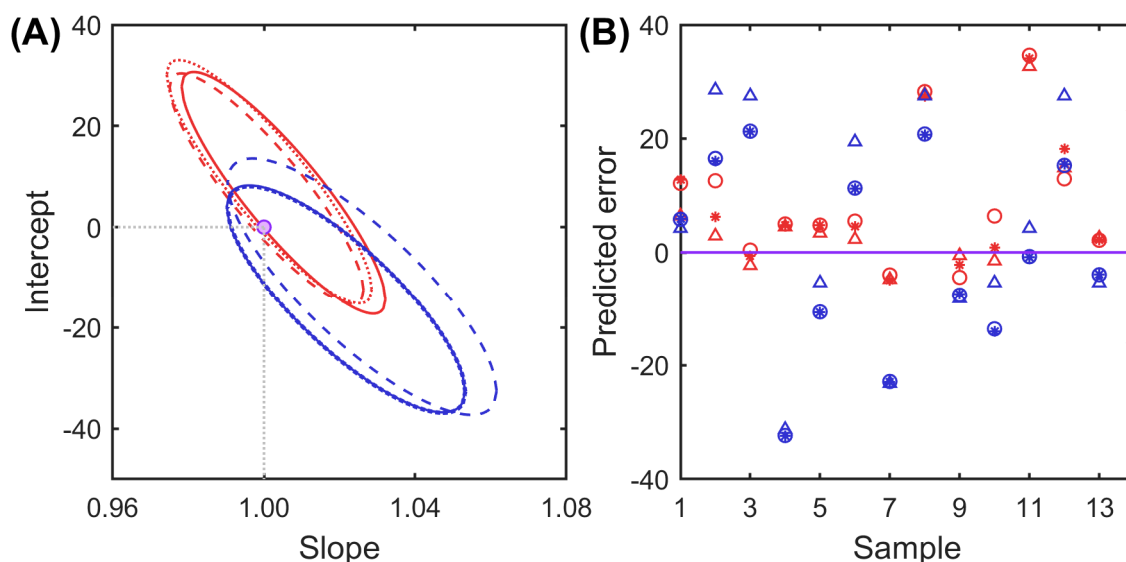
Figure 4. (**A**). Elliptical joint of confidence region plots obtained for THY (blue lines) and CAR (red lines) with the different models: raw and mean-cantering (solid lines), first derivative (dotted lines), and second derivative (dashed lines), where the point (0,1) is the ideal point. (**B**). Prediction errors obtained for THY (blue markers) and CAR (red markers) with the different models: raw and mean-cantering (circles), first derivative (asterisks), and second derivative (triangles).

The elliptical domains obtained for the analytes using different models visibly encompass the theoretically expected point (1,0) for slope and intercept, respectively, demonstrating the accuracy of the proposed methodologies. Nevertheless, the domains obtained for CAR determination draw near the ideal point borderline, with the second derivative-based methodology yielding the most satisfactory results. On the other hand, for THY, the most centered ellipse was achieved using the first derivative data. Last, it is worth highlighting that the residuals show a random pattern, indicating the lack of correlation between samples (Figure 4B).

Based on these observations, when analyzing EO samples, the first derivative-based model is employed for THY, while for CAR, second derivative data are preferred.

3.3. Analytical Figures of Merit

The analytical figures of merits (AFOMs) were estimated to comprehensively describe the analytical performance of the proposed method. As stated, the first derivative-based model was employed for THY, while for CAR, the second derivative data were preferred.

Sensitivity (SEN), analytical sensitivity (γ), limit of detection (LOD), and limit of quantitation (LOQ) for each analyte were estimated according to [58] and are summarized in Table 2.

Table 2. Analytical figures of merits.

AFOM	THY	CAR
SEN (A/μM)	3.5×10^{-13}	1.3×10^{-14}
γ (μM)	293.1	18.8
LOD (μM)	7.4–13.8	9.8–13.6
LOQ (μM)	22.1–41.4	29.5–40.8

As stated in Table 2, the LOD figures estimated for the THY and CAR reached values as low as 7.4 and 9.8 μM, respectively. Although these values slightly exceed those found in the literature for simultaneous analyte determination using an electrochemical approach, it is crucial to note that the proposed methodology does not require modifications to the electrode surface or complex data analysis. For instance, Kowalcze and Jakubowska [44] reported the simultaneous determination of eugenol, THY, and CAR using DPV combined with PLS at a boron-doped diamond electrode, achieving LODs around 0.1 μM and REP below 5.1%. Meanwhile, Tonello et al. [43] detailed the determination of EUG, THY, and CAR using SWV combined with ANN at GCE, obtaining similar REP values to the proposed method, albeit with a higher LOD for both analytes (16 μM).

3.4. Analysis of OEO and TEO

The TEO and OEO samples were characterized through GC-MS, and THY and CAR content were determined and comprehensively compared with those obtained in this work. The chromatographic profiles of TEO and OEO are shown in Figure S4 (Supplementary Materials).

GC-MS analyses revealed that the TEO and OEO samples primarily comprise oxygenated and hydrocarbon monoterpenes and sesquiterpenes. Among the oxygenated monoterpenes, THY and CAR emerged as the predominant compounds. Specifically, in TEO, phenolic monoterpenes constituted over 40%, with approximately 95% being THY. On the other hand, OEO exhibited a content exceeding 50%, with c.a. 90% attributed to CAR within the phenolic monoterpenes category. Table 3 shows the predicted concentrations of THY and CAR obtained with the GC-MS methodology and those obtained with the developed electrochemical method. Moreover, the predicted concentrations of CAR and THY in samples obtained for GC-MS, i.e., prior to dilution, are displayed.

Table 3. Predictive concentrations of THY and CAR in TEO and OEO samples through GC-MS and the proposed electrochemical (EQ) method.

Sample	THY			CAR			Content in Sample	
	GC-MS (μM)	EQ (μM)	R%	GC-MS (μM)	EQ (μM)	R%	THY (%*w/v*)	CAR (%*w/v*)
OEO 1	12.0	18.9	157.5	536.0	560.4	104.5	1.4	42.0
OEO 2	12.0	17.9	149.1	843.0	874.8	103.8	1.3	65.6
OEO 3	397.0	371.3	93.5	843.0	818.1	97.0	27.8	61.3
OEO 4	390.0	332.4	85.2	1270.0	1200.0	94.5	24.9	90
TEO 5	288.0	235.4	81.7	13.0	9.1	70.0	17.7	0.7
TEO 6	434.0	462.6	106.6	13.0	13.3	102.3	34.7	1.0
TEO 7	505.0	509.2	100.8	501.0	488.8	97.6	38.2	36.7
TEO 8	856.0	777.3	90.8	501.0	537.7	107.3	58.3	40.3
$\overline{R}$% [a]		108.2			97.1			
REP% [b]		5.6			4.3			

[a] $\overline{R}$% = average percentage of recovery given in %. [b] REP% = relative error of prediction given in %.

The recoveries (R%) and REP% of the predicted analyte concentrations in TEO and OEO obtained with the proposed method were estimated considering GC-MS as the reference method.

The initial observation deserving attention is that OEO 1 and OEO 2 exhibit predicted THY concentrations borderline the LOD upper limit. Likewise, TEO5 and TEO6 predicted CAR concentrations falling within the range defined by the LOD and LOQ. Consequently, it is unsurprising that these samples display the most significant differences in predicted levels. Notably, these samples correspond to those for which THY and CAR were not added; hence, the predicted concentration refers to the TEO and OEO basal concentration. It is worth emphasizing that these concentrations, within the LOD and LOQ range, may contribute to the observed prediction disparities. However, it should be noted that these samples underwent a dilution process first in EtOH and then in ACN to facilitate measurements. Hence, there is an opportunity for refinement in the sample preparation process to achieve concentrations falling within the quantitative range of prediction. Slight adjustments in the preparation protocol could yield data points that are more aligned with the intended quantitative analysis. Notably, these samples were those for which the THY and CAR concentrations were the EO basal concentration, i.e., not spiked samples.
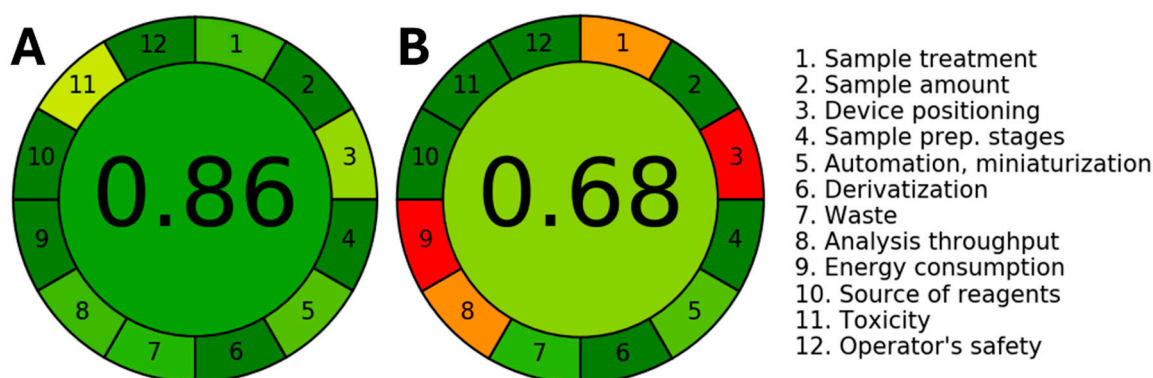
To assert the accuracy, the R% values were statistically evaluated against the ideal value of 100% using a *t*-test. The null hypothesis posits that the average experimental R% is not significantly different from the ideal value. For this, an experimental t_{exp} value was estimated for each analyte and compared to a critical $t_{(\alpha, \upsilon)}$ value at level α and $\upsilon = I-1$ degree of freedom (with *I* being the number of validation samples). Considering a level of $\alpha = 0.05$, the t_{exp} (0.79552 and 0.68796 for THY and CAR, respectively) were lower than the critical $t_{(0.05,7)} = 2.3677$, indicating that the experimental recoveries are not statistically different from 100%. Therefore, the accuracy of the method was asserted.

At this point, it is noteworthy that all calibration and validation samples were prepared in an organic medium rather than the EO matrices. This procedure was performed due to the unavailability of OEO and TEO without THY and CAR content. However, the satisfactory results confirm the absence of signal interference in the EO matrix, demonstrating the practical suitability of the proposed methodology in real samples.

3.5. Greenness Evaluation

To provide deeper insights into the advantages of the proposed methodology, the sustainability of the method was quantitatively evaluated through the GREEnness metric approach previously reported by Pena-Pereira et al. in 2020 [54]. This metric assesses the greenness of a method by assigning a score to the analytical procedure on a scale from 0 to 1, based on adherence to the 12 principles of green analytical chemistry. A higher overall score indicates a greener methodology, reflecting a more environmentally sustainable approach.

The score of the proposed method was obtained and compared with the one obtained for the GC-MS-based approach. Figure 5 shows the pictograms depicting the overall scores and the performance of the individual criterion according to a color scale obtained for EQ and GC-MS methodologies.

1. Sample treatment
2. Sample amount
3. Device positioning
4. Sample prep. stages
5. Automation, miniaturization
6. Derivatization
7. Waste
8. Analysis throughput
9. Energy consumption
10. Source of reagents
11. Toxicity
12. Operator's safety

Figure 5. Green assessment of the (**A**) PtME-based method developed to determine THY and CAR in TEO and OEO and (**B**) the GC-MS method using the AGREE metric.

In the case of the proposed PtME-based method, the lowest score was obtained for the usage of organic solvent (score 11). However, the miniaturized size of the electrodes aids in diminishing the volume of solvent required for the measurements. Notwithstanding, most of the individual scores highly satisfied the criterion of greenness, achieving an overall score of 0.86, which is significantly better than those obtained for the reference method (GC-MS, 0.68). This result endorses the sustainability of the proposed method, shedding light on the fact that the methodology aligns with the criteria of green analytical chemistry.

Many scientific publications have demonstrated the relevance of the simultaneous determination of THY and CAR. The most relevant ones are summarized in Table S3 (Supplementary Materials). As can be seen, most of the approaches are based on separative techniques (gas or liquid chromatography), offering satisfactory results in terms of LOD and recovery rates in different samples. However, they are time-consuming (3–30 min), require several steps of sample pretreatment, and generate a large amount of waste. Since these characteristics do not align well with the twelve principles of green chemistry, these methods cannot be considered environmentally sustainable, as demonstrated by the low score obtained with AGREE evaluation (AGREE evaluation in Table S3 (Supplementary Materials)).

On the other hand, performing simultaneous determination of THY and CAR usually requires multivariate calibration tools due to the high overlap between electrochemical signals. It has been demonstrated that implementing these approaches aids in reducing sample pretreatment, time, and waste, which are the primary goals of the GAC. In the literature, only two methods are found in which PLS and ANN were used to determine THY and CAR in honey samples without requiring sample pretreatment. These methods allow for the fast and successful determination of the analytes, showing good recovery figures; however, the LOD determination is estimated for a univariate calibration model (not recommended), and in the case of the PLS model, many latent variables are used, which may lead to a model overfitting.

To the best of our knowledge, the method proposed in this work is the first reporting of the simultaneous determination of THY and CAR in essential oil samples using PLS models with minimal data pretreatment. Despite the obtained LODs being higher than those obtained by other methods [60–62] (see Table S3 in Supplementary Materials), the THY and CAR content in TEO and OEO is much higher than the LOD. In addition, this method stands out for its simplicity since it requires no sample pretreatment (only dilution in supporting electrolyte), a small amount of sample needed, low waste, and low time consumption, all the characteristics within the GAC framework. All these accomplishments assess the suitability of the unmodified PtME in determining THY and CAR in essential oils in a sustainable manner.

4. Conclusions

The combination of PtME and multivariate calibration models has demonstrated a remarkably efficient, straightforward, and sustainable strategy for simultaneously determining THY and CAR in thyme and oregano essential oil. Utilizing micro-sized electrodes leverages the potential of the electrochemical-based approaches by enhancing the analytical performance of the methods while requiring minimal sample volumes. The advantages mentioned above outweigh the disadvantages associated with using microelectrodes, including low currents and mechanical fragility, among others.

The excellent reproducibility of acquired SW voltammograms was confirmed through PLS models applied to raw and pretreated data, yielding satisfactory results. However, a simple preprocessing data protocol was adopted, pursuing an improvement in the analytical performance in a parsimonious manner. The first derivative and mean-centering were implemented as preprocessing for THY determination, while CAR determination was accomplished with mean-centered second derivatives.

The predictive capability of the method was asserted by comparing the results obtained with those obtained with GC-MS, which is considered the reference method. The results

underscore the suitability of the method for determining THY and CAR (two isomers with highly overlapped electrochemical signals) at low concentrations (LOD ~7.6 μmol L^{-1}) with REPs below 5.6% in essential oils. Last, it is noteworthy that the method's environmental sustainability was asserted using the AGREE metric, meeting the criteria of green analytical chemistry and highlighting its eco-friendly nature.

Supplementary Materials: The following supporting information can be downloaded at: https://www.mdpi.com/article/10.3390/chemosensors12090197/s1, Table S1. Concentrations of THY and CAR used in the calibration and validation sets; Table S2. Volumes of standard stock solution used for spiked EO sample set (total volume=5.00 mL); Table S3. Comparison between the proposed electrochemical method and others found in the literature; Figure S1. Cyclic voltammograms at different v (from 5 to 250 mV.s^{-1}) recorded in ACN + 0.1 M TBAP at Pt macroelectrode for (a) THY concentration of 1.0×10^{-3} M and (b) CAR concentration of 1.0×10^{-3} M. Plots of $I_{p,a}$ vs $v^{\frac{1}{2}}$, for (c) THY and (d) CAR; Figure S2. (a) Cyclic voltammogram recorded for 3 mM of Fc in ACN + 0.1 M TBAP solution at PtME disk. Scan rate: 5 mV s^{-1}. (b) Chronoamperograms recorded after applying a double potential step from 0 to 0.6 V during 5 s at PtME disk; Figure S3. SW voltammograms recorded for 1.0×10^{-3} M of THY + CAR in ACN + 0.1 M TBAP solution at PtME disk (black line) and Pt macroelectrode (red line). Square wave conditions were: ΔE_{SW} = 0.025 V, ΔEs = 0.005 V, and f = 15 Hz; Figure S4. GC-MS profiles recorded for (a) TEO and (b) OEO.

References

1. Arafa, W.M.; Abolhadid, S.M.; Moawad, A.; Abdelaty, A.S.; Moawad, U.K.; Shokier, K.A.M.; Shehata, O.; Gadelhaq, S.M. Thymol efficacy against coccidiosis in pigeon (*Columba livia domestica*). *Prev. Vet. Med.* **2020**, *176*, 104914. [CrossRef] [PubMed]
2. Boye, A.; Addo, J.K.; Acheampong, D.O.; Thomford, A.K.; Asante, E.; Amoaning, R.E.; Kuma, D.N. The hydroxyl moiety on carbon one (C1) in the monoterpene nucleus of thymol is indispensable for anti-bacterial effect of thymol. *Heliyon* **2020**, *6*, e03492. [CrossRef] [PubMed]
3. Cai, R.; Zhang, M.; Cui, L.; Yuan, Y.; Yang, Y.; Wang, Z.; Yue, T. Antibacterial activity and mechanism of thymol against Alicyclobacillus acidoterrestris vegetative cells and spores. *LWT* **2019**, *105*, 377–384. [CrossRef]

4. Gavliakova, S.; Biringerova, Z.; Buday, T.; Brozmanova, M.; Calkovsky, V.; Poliacek, I.; Plevkova, J. Antitussive effects of nasal thymol challenges in healthy volunteers. *Respir. Physiol. Neurobiol.* **2013**, *187*, 104–107. [CrossRef]

5. Marchese, A.; Orhan, I.E.; Daglia, M.; Barbieri, R.; Di Lorenzo, A.; Nabavi, S.F.; Gortzi, O.; Izadi, M.; Nabavi, S.M. Antibacterial and antifungal activities of thymol: A brief review of the literature. *Food Chem.* **2016**, *210*, 402–414. [CrossRef]

6. Rezaeinasab, M.; Benvidi, A.; Gharaghani, S.; Abbasi, S.; Zare, H.R. Electrochemical investigation of the inhibition effect of carvacrol on xanthine oxidase activity merging with theoretical studies. *Process Biochem.* **2019**, *83*, 86–95. [CrossRef]

7. Guan, X.; Li, X.; Yang, X.; Yan, J.; Shi, P.; Ba, L.; Cao, Y.; Wang, P. The neuroprotective effects of carvacrol on ischemia/reperfusion-induced hippocampal neuronal impairment by ferroptosis mitigation. *Life Sci.* **2019**, *235*, 116795. [CrossRef]

8. Khan, I.; Bhardwaj, M.; Shukla, S.; Min, S.-H.; Choi, D.K.; Bajpai, V.K.; Huh, Y.S.; Kang, S.C. Carvacrol inhibits cytochrome P450 and protects against binge alcohol-induced liver toxicity. *Food Chem. Toxicol.* **2019**, *131*, 110582. [CrossRef]

9. Gursul, S.; Karabulut, I.; Durmaz, G. Antioxidant efficacy of thymol and carvacrol in microencapsulated walnut oil triacylglycerols. *Food Chem.* **2019**, *278*, 805–810. [CrossRef]

10. Mechergui, K.; Jaouadi, W.; Coelho, J.P.; Khouja, M.L. Effect of harvest year on production, chemical composition and antioxidant activities of essential oil of oregano (*Origanum vulgare* subsp *glandulosum* (Desf.) Ietswaart) growing in North Africa. *Ind. Crops Prod.* **2016**, *90*, 32–37. [CrossRef]

11. Verma, R.S.; Padalia, R.C.; Goswami, P.; Upadhyay, R.K.; Singh, V.R.; Chauhan, A.; Tiwari, A.K. Assessing productivity and essential oil quality of Himalayan thyme (*Thymus linearis* Benth.) in the subtropical region of north India. *Ind. Crops Prod.* **2016**, *94*, 557–561. [CrossRef]

12. Cui, H.; Zhang, C.; Li, C.; Lin, L. Antibacterial mechanism of oregano essential oil. *Ind. Crops Prod.* **2019**, *139*, 111498. [CrossRef]

13. Alsaraf, S.; Hadi, Z.; Al-Lawati, W.M.; Al Lawati, A.A.; Khan, S.A. Chemical composition, in vitro antibacterial and antioxidant potential of Omani Thyme essential oil along with in silico studies of its major constituent. *J. King Saud Univ. Sci.* **2020**, *32*, 1021–1028. [CrossRef]

14. Cruz-Tirado, J.P.; Barros Ferreira, R.S.; Lizárraga, E.; Tapia-Blácido, D.R.; Silva, N.C.C.; Angelats-Silva, L.; Siche, R. Bioactive Andean sweet potato starch-based foam incorporated with oregano or thyme essential oil. *Food Packag. Shelf Life* **2020**, *23*, 100457. [CrossRef]

15. Lee, S.; Kim, H.; Beuchat, L.R.; Kim, Y.; Ryu, J.-H. Synergistic antimicrobial activity of oregano and thyme thymol essential oils against *Leuconostoc citreum* in a laboratory medium and tomato juice. *Food Microbiol.* **2020**, *90*, 103489. [CrossRef]

16. Hajimehdipoor, H.; Shekarchi, M.; Khanavi, M.; Adib, N.; Amri, M. A validated high performance liquid chromatography method for the analysis of thymol and carvacrol in *Thymus vulgaris* L. volatile oil. *Pharmacogn. Mag.* **2010**, *6*, 154–158. [CrossRef]

17. Beena; Kumar, D.; Rawat, D.S. Synthesis and antioxidant activity of thymol and carvacrol based Schiff bases. *Bioorganic Med. Chem. Lett.* **2013**, *23*, 641–645. [CrossRef]

18. Sarikurkcu, C.; Zengin, G.; Oskay, M.; Uysal, S.; Ceylan, R.; Aktumsek, A. Composition, antioxidant, antimicrobial and enzyme inhibition activities of two *Origanum vulgare* subspecies (subsp. *vulgare* and subsp. *hirtum*) essential oils. *Ind. Crops Prod.* **2015**, *70*, 178–184. [CrossRef]

19. Alekseeva, L.I. Determining thymol and carvacrol by reversed-phase high-performance liquid chromatography. *Pharm. Chem. J.* **2009**, *43*, 665–667. [CrossRef]

20. Ghaedi, M.; Roosta, M.; Khodadoust, S.; Daneshfar, A. Application of Optimized Vortex-Assisted Surfactant-Enhanced DLLME for Preconcentration of Thymol and Carvacrol, and Their Determination by HPLC-UV: Response Surface Methodology. *J. Chromatogr. Sci.* **2015**, *53*, 1222–1231. [CrossRef]

21. Roosta, M.; Ghaedi, M.; Daneshfar, A.; Sahraei, R. Ultrasound assisted microextraction-nano material solid phase dispersion for extraction and determination of thymol and carvacrol in pharmaceutical samples: Experimental design methodology. *J. Chromatogr. B* **2015**, *975*, 34–39. [CrossRef] [PubMed]

22. Ghiasvand, A.; Dowlatshah, S.; Nouraei, N.; Heidari, N.; Yazdankhah, F. A solid-phase microextraction platinized stainless steel fiber coated with a multiwalled carbon nanotube-polyaniline nanocomposite film for the extraction of thymol and carvacrol in medicinal plants and honey. *J. Chromatogr. A* **2015**, *1406*, 87–93. [CrossRef] [PubMed]

23. Fiori, G.M.L.; Bonato, P.S.; Pereira, M.P.M.; Contini, S.H.T.; Pereira, A.M.S. Determination of thymol and carvacrol in plasma and milk of dairy cows using solid-phase microextraction. *J. Braz. Chem. Soc.* **2013**, *24*, 837–846. [CrossRef]

24. Ares, A.M.; Nozal, M.J.; Bernal, J.L.; Bernal, J. Simultaneous determination of carvacrol and thymol in bee pollen by using a simple and efficient solvent extraction method and gas chromatography-mass spectrometry. *J. Pharm. Biomed. Anal.* **2020**, *181*, 113124. [CrossRef]

25. Jiménez-Salcedo, M.; Tena, M.T. Determination of cinnamaldehyde, carvacrol and thymol in feedstuff additives by pressurized liquid extraction followed by gas chromatography–mass spectrometry. *J. Chromatogr. A* **2017**, *1487*, 14–21. [CrossRef]

26. Pavela, R.; Bartolucci, F.; Desneux, N.; Lavoir, A.-V.; Canale, A.; Maggi, F.; Benelli, G. Chemical profiles and insecticidal efficacy of the essential oils from four Thymus taxa growing in central-southern Italy. *Ind. Crops Prod.* **2019**, *138*, 111460. [CrossRef]

27. Lemos, M.F.; Lemos, M.F.; Pacheco, H.P.; Guimarães, A.C.; Fronza, M.; Endringer, D.C.; Scherer, R. Seasonal variation affects the composition and antibacterial and antioxidant activities of *Thymus vulgaris*. *Ind. Crops Prod.* **2017**, *95*, 543–548. [CrossRef]

28. Kasiotis, K.M.; Tzouganaki, Z.D.; Machera, K. Chromatographic determination of monoterpenes and other acaricides in honeybees: Prevalence and possible synergies. *Sci. Total Environ.* **2018**, *625*, 96–105. [CrossRef]

29. Kiyanpour, V.; Fakhari, A.R.; Alizadeh, R.; Asghari, B.; Jalali-Heravi, M. Multivariate optimization of hydrodistillation-headspace solvent microextraction of thymol and carvacrol from *Thymus transcaspicus*. *Talanta* **2009**, *79*, 695–699. [CrossRef]

30. Chang, X.; Sun, P.; Ma, Y.; Han, D.; Zhao, Y.; Bai, Y.; Zhang, D.; Yang, L. A New Method for Determination of Thymol and Carvacrol in Thymi herba by Ultraperformance Convergence Chromatography (UPC2). *Molecules* **2020**, *25*, 502. [CrossRef]

31. Welch, C.J.; Wu, N.; Biba, M.; Hartman, R.; Brkovic, T.; Gong, X.; Helmy, R.; Schafer, W.; Cuff, J.; Pirzada, Z.; et al. Greening analytical chromatography. *TrAC Trends Anal. Chem.* **2010**, *29*, 667–680. [CrossRef]

32. Yáñez-Sedeño, P.; Campuzano, S.; Pingarrón, J.M. Electrochemical (bio)sensors: Promising tools for green analytical chemistry. *Curr. Opin. Green Sustain. Chem.* **2019**, *19*, 1–7. [CrossRef]

33. Michelitsch, A.; Rittmannsberger, A.; Hüfner, A.; Rückert, U.; Likussar, W. Determination of isopropylmethylphenols in black seed oil by differential pulse voltammetry. *Phytochem. Anal.* **2004**, *15*, 320–324. [CrossRef] [PubMed]

34. Fuentes, F.G.; Gil, M.Á.L.; Mendoza, S.; Escarpa, A. Electrochemical Screening of Biomarkers in Chemotype Mexican Oregano Oils on Single-Walled Carbon Nanotubes Screen-Printed Electrodes. *Electroanalysis* **2011**, *23*, 2212–2216. [CrossRef]

35. Robledo, S.N.; Pierini, G.D.; Nieto, C.H.D.; Fernández, H.; Zon, M.A. Development of an electrochemical method to determine phenolic monoterpenes in essential oils. *Talanta* **2019**, *196*, 362–369. [CrossRef]

36. Esteban, M.; Ariño, C.; Díaz-Cruz, J.M. Chemometrics in Electrochemistry. In *Reference Module in Chemistry, Molecular Sciences and Chemical Engineering*; Elsevier: Amsterdam, The Netherlands, 2019.

37. Robledo, S.N.; Zachetti, V.G.L.; Zon, M.A.; Fernández, H. Quantitative determination of tocopherols in edible vegetable oils using electrochemical ultra-microsensors combined with chemometric tools. *Talanta* **2013**, *116*, 964–971. [CrossRef]

38. Tesio, A.Y.; Robledo, S.N.; Granero, A.M.; Fernández, H.; Zon, M.A. Simultaneous electroanalytical determination of luteolin and rutin using artificial neural networks. *Sens. Actuators B Chem.* **2014**, *203*, 655–662. [CrossRef]

39. Pierini, G.D.; Pistonesi, M.F.; Di Nezio, M.S.; Centurión, M.E. A pencil-lead bismuth film electrode and chemometric tools for simultaneous determination of heavy metals in propolis samples. *Microchem. J.* **2016**, *125*, 266–272. [CrossRef]

40. Granero, A.M.; Pierini, G.D.; Robledo, S.N.; Di Nezio, M.S.; Fernández, H.; Zon, M.A. Simultaneous determination of ascorbic and uric acids and dopamine in human serum samples using three-way calibration with data from square wave voltammetry. *Microchem. J.* **2016**, *129*, 205–212. [CrossRef]

41. Kumar, N.; Bansal, A.; Sarma, G.S.; Rawal, R.K. Chemometrics tools used in analytical chemistry: An overview. *Talanta* **2014**, *123*, 186–199. [CrossRef]

42. Kumar, K. Partial Least Square (PLS) Analysis. *Resonance* **2021**, *26*, 429–442. [CrossRef]

43. Tonello, N.; Moressi, M.B.; Robledo, S.N.; D'Eramo, F.; Marioli, J.M. Square wave voltammetry with multivariate calibration tools for determination of eugenol, carvacrol and thymol in honey. *Talanta* **2016**, *158*, 306–314. [CrossRef] [PubMed]

44. Kowalcze, M.; Jakubowska, M. Multivariate approach in voltammetric identification and simultaneous determination of eugenol, carvacrol, and thymol on boron-doped diamond electrode. *Monatshefte Für Chem. Chem. Mon.* **2019**, *150*, 991–1002. [CrossRef]

45. Darío Pierini, G.; Andrés Bortolato, S.; Noel Robledo, S.; Raquel Alcaraz, M.; Fernández, H.; Casimiro Goicoechea, H.; Alicia Zon, M. Second-order electrochemical data generation to quantify carvacrol in oregano essential oils. *Food Chem.* **2022**, *368*, 130840. [CrossRef]

46. Stulík, K.; Amatore, C.; Holub, K.; Marecek, V.; Kutner, W. Microelectrodes. Definitions, characterization, and applications (Technical report). *Pure Appl. Chem.* **2000**, *72*, 1483. [CrossRef]

47. Marriott, P.J.; Shellie, R.; Cornwell, C. Gas chromatographic technologies for the analysis of essential oils. *J. Chromatogr. A* **2001**, *936*, 1–22. [CrossRef]

48. Robledo, S.N.; Tesio, A.Y.; Ceballos, C.D.; Zon, M.A.; Fernández, H. Electrochemical ultra-micro sensors for the determination of synthetic and natural antioxidants in edible vegetable oils. *Sens. Actuators B Chem.* **2014**, *192*, 467–473. [CrossRef]

49. Wang, Y.; Rogers, E.I.; Compton, R.G. The measurement of the diffusion coefficients of ferrocene and ferrocenium and their temperature dependence in acetonitrile using double potential step microdisk electrode chronoamperometry. *J. Electroanal. Chem.* **2010**, *648*, 15–19. [CrossRef]

50. Shoup, D.; Szabo, A. Chronoamperometric current at finite disk electrodes. *J. Electroanal. Chem.* **1982**, *140*, 237–245. [CrossRef]

51. Brereton, R.G. Multilevel Multifactor Designs for MultivariateCalibration. *Analyst* **1997**, *122*, 1521–1529. [CrossRef]

52. *MATLAB 9.4.0*; The MathWorks Inc.: Natick, MA, USA, 2018.

53. Olivieri, A.C.; Goicoechea, H.C.; Iñón, F.A. MVC1: An integrated MatLab toolbox for first-order multivariate calibration. *Chemom. Intell. Lab. Syst.* **2004**, *73*, 189–197. [CrossRef]

54. Pena-Pereira, F.; Wojnowski, W.; Tobiszewski, M. AGREE—Analytical GREEnness Metric Approach and Software. *Anal. Chem.* **2020**, *92*, 10076–10082. [CrossRef] [PubMed]

55. Bard, A.J.; Faulkner, L.R.; White, H.S. *Electrochemical Methods: Fundamentals and Applications*, New York: Wiley, 2001, 2nd ed. *Russ. J. Electrochem.* **2002**, *38*, 1364–1365. [CrossRef]

56. Orozco, J.; Fernández-Sánchez, C.; Jiménez-Jorquera, C. Ultramicroelectrode Array Based Sensors: A Promising Analytical Tool for Environmental Monitoring. *Sensors* **2010**, *10*, 475–490. [CrossRef]

57. Esteban, M.; Ariño-Blasco, M.C.; Díaz-Cruz, J.M. 4.01-Chemometrics in Electrochemistry. In *Comprehensive Chemometrics*, 2nd ed.; Brown, S., Tauler, R., Walczak, B., Eds.; Elsevier: Oxford, UK, 2020; pp. 1–31.

58. Olivieri, A.C. *Introduction to Multivariate Calibration: A Practical Approach*; Springer: Berlin/Heidelberg, Germany, 2018.

59. Díaz-Cruz, J.M.; Esteban, M.; Ariño, C. Multivariate Calibration. In *Chemometrics in Electroanalysis*; Díaz-Cruz, J.M., Esteban, M., Ariño, C., Eds.; Springer International Publishing: Cham, Switzerland, 2019; pp. 87–129.

60. Bernal, J.; Nozal, M.J.; Bernal, J.L.; Ares, A.M. Determination of Carvacrol and Thymol in Honey by Using a Simple and Efficient Headspace-Gas Chromatography-Mass Spectrometry Method. *Food Anal. Methods* **2020**, *13*, 2138–2146. [CrossRef]

61. Kasiri, E.; Haddadi, H.; Javadian, H.; Asfaram, A. Highly effective pre-concentration of thymol and carvacrol using nano-sized magnetic molecularly imprinted polymer based on experimental design optimization and their trace determination in summer savoury, Origanum majorana and Origanum vulgare extracts. *J. Chromatogr. B* **2021**, *1182*, 122941. [CrossRef]

62. Cantalapiedra, A.; Gismera, M.J.; Sevilla, M.T.; Procopio, J.R. Sensitive and Selective Determination of Phenolic Compounds from Aromatic Plants Using an Electrochemical Detection Coupled with HPLC Method. *Phytochem. Anal.* **2014**, *25*, 247–254. [CrossRef]